Journal Pre-proof

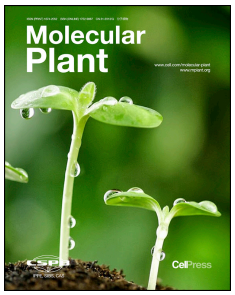


# HASTY modulates miRNA biogenesis by linking pri-miRNA transcription and processing

Damian A. Cambiagno, Axel J. Giudicatti, Agustin L. Arce, Delfina Gagliardi, Lei Li, Wei Yuan, Derek S. Lundberg, Detlef Weigel, Pablo A. Manavella

PII: S1674-2052(20)30450-0
DOI: https://doi.org/10.1016/j.molp.2020.12.019
Reference: MOLP 1069

To appear in: *MOLECULAR PLANT*
Accepted Date: 28 December 2020

Please cite this article as: **Cambiagno D.A., Giudicatti A.J., Arce A.L., Gagliardi D., Li L., Yuan W., Lundberg D.S., Weigel D., and Manavella P.A.** (2021). HASTY modulates miRNA biogenesis by linking pri-miRNA transcription and processing. Mol. Plant. doi: https://doi.org/10.1016/j.molp.2020.12.019.

# HASTY modulates miRNA biogenesis by linking pri-miRNA transcription and processing

Damian A. Cambiagno[1], Axel J. Giudicatti[1], Agustin L. Arce[1], Delfina Gagliardi[1], Lei Li[2], Wei Yuan[2], Derek S. Lundberg[2], Detlef Weigel[2], Pablo A. Manavella[1*]

[1] Instituto de Agrobiotecnología del Litoral (CONICET-UNL), Cátedra de Biología Celular y Molecular, Facultad de Bioquímica y Ciencias Biológicas, Universidad Nacional del Litoral, 3000 Santa Fe, Argentina.

[2] Department of Molecular Biology, Max Planck Institute for Developmental Biology, 72076 Tübingen, Germany

*To whom correspondence should be addressed. E-mail pablomanavella@ial.santafe-conicet.gov.ar

## Short Summary

HASTY, the plant orthologue of human EXPORTIN5, was proposed to export miRNAs from the nucleus to the cytoplasm, although this function was long disputed. This study shows that HASTY, far from acting as a miRNA cargo protein, promotes miRNA biogenesis stabilizing a complex between DCL1 and Mediator at MIRNA loci.

## Abstract

Post-transcriptional gene silencing mediated by microRNAs (miRNAs) modulates numerous developmental and stress response pathways. For the last two decades, HASTY (HST), the ortholog of human Exportin-5, has been considered as a candidate protein that exports plant miRNAs from the nucleus to the cytoplasm. Here, we report HST functions in the miRNA pathway independent of its cargo-exporting activity in *Arabidopsis*. We found that *Arabidopsis* mutants with impaired HST shuttling present normal subcellular distribution of miRNAs. Interestingly, protein-protein interaction and microscopy assays showed that HST directly interacts with the microprocessor core component DCL1 through its N-terminal domain. Moreover, mass-spectrometry analysis revealed that HST also interacts, independently of its N-terminal domain, with the mediator complex subunit MED37. Further experiments

showed that HST could act as a scaffold to facilitate the recruitment of DCL1 to genomic *MIRNA* loci by stabilizing the DCL1-MED37 complex, which in turn promotes the transcription and proper processing of pri-miRNAs. In summary, our results suggest that HST is likely associated with the formation of the miRNA biogenesis complex at *MIRNA* genes, promoting the transcription and processing of pri-miRNAs, rather than with the direct export of processed miRNAs from the nucleus.

## Introduction

Gene silencing by microRNAs (miRNAs) is an essential mechanism of posttranscriptional gene regulation during both the development and stress responses in plants (Manavella et al., 2019; Rogers and Chen, 2013). MiRNAs originate from genomic *MIRNA* loci. RNA polymerase II (RNAPII), together with the elongator and mediator complexes, transcribes them to produce primary miRNA transcripts (pri-miRNAs) (Fang et al., 2015; Kim et al., 2011). DICER-LIKE 1 (DCL1), along with accessory proteins, functions as microprocessor to generate mature miRNA duplexes from the pri-miRNAs (Achkar et al., 2016). Transcription of *MIRNA* genes and the further processing of the pri-miRNAs are linked processes as most of the biogenesis factors are recruited to the *MIRNA* loci early during transcription (Fang et al., 2015; Wang et al., 2019). After processing, mature miRNAs are loaded into ARGONAUTE1 (AGO1), leading the silencing of targeted mRNAs in microsomal and membrane-bound polysomes (Li et al., 2016; Rogers and Chen, 2013). In plants, miRNA processing takes place entirely in the nucleus.

HASTY (HST) was first described as a factor regulating the timing of juvenile to adult and flowering transition, two developmental processes in which miRNAs play key roles (Telfer and Poethig, 1998). HST was classified as a member of the karyopherin family (Bollman et al., 2003). Karyopherins are transport receptors required for export or import of cargoes through the nuclear pore complex. Translocation of cargoes by karyopherin depends on small GTPases proteins called RAS-RELATED NUCLEAR PROTEIN (RAN). The association of karyopherins with RAN-GTP promotes nuclear export, while the GTP hydrolysis leads to the dissociation of cargoes in the cytoplasm (Meier and Brkljacic, 2010; Merkle, 2011). *Arabidopsis thaliana* encodes four RAN-like

proteins among 93 GTP-binding proteins. RAN1, RAN2, and RAN3 have over 95% identity with each other, while RAN4 is divergent with an identity to the other three near 65% (Vernoud et al., 2003). The *A. thaliana* genome encodes 17 karyopherins, of which four are related to the miRNA pathway. TRANSPORTIN 1 participates in AGO1-miRNA loading but not miRNA nuclear export (Cui et al., 2016; Wang et al., 2011a); KETCH1 allows HYL1 translocation to the nucleus (Zhang et al., 2017b); EXPORTIN-1 (EXP1/XPO1) aids AGO1 nucleus to cytoplasm movement (Bologna et al., 2018); and HST modulates miRNA accumulation by an unknown mechanism (Bollman et al., 2003; Park et al., 2005).

HST has been implicated in miRNA biogenesis based on genetics, with reduced levels of some miRNAs in *hst* mutants (Lang et al., 2018; Park et al., 2005; Zhang et al., 2017a). HST is the plant ortholog of exportin 5 (EXP5/XPO5), and by analogy with the animal system, HST was proposed to export miRNA from the nucleus to cytoplasm in plants (Brownawell and Macara, 2002). EXP5 also acts independently of its exporting activity by enhancing pri-miRNA processing efficiency of DROSHA/DGCR8 microprocessor (Wang et al., 2020). Importantly, the assumption of HST being a miRNA exporter was based on expected functional homology between organisms, but it was not supported by experimental data, as the subcellular distribution of miRNAs between nucleus and cytoplasm is not altered in *hst* mutants (Park et al., 2005). Recently, it was found that plant AGO1 enters the nucleus, where it is loaded with mature miRNAs, before translocating to the cytoplasm in a process assisted by NUP1/THP1 (Bologna et al., 2018, Zhang et al., 2020).

Here we show that the ability of HST to mediate cargo export can be dissociated from its role in the miRNA pathway, as the first, but not the second, is RAN1-dependent. We found that RAN1 is required for HST movement from the nucleus to the cytoplasm while IMPORTIN ALPHA ISOFORM 2 (IMPA-2) controls HST shuttling into the nucleus. However, neither of these proteins appeared necessary for miRNA transport out of the nucleus. Importantly, we found that HST is not directly involved in pri-miRNAs processing, as its human ortholog. Instead, HST acts as a scaffold allowing the formation of a protein complex between DCL1 and MED37, which in turn is required for DCL1 recruitment to *MIR* genes and further processing of the pri-miRNAs.

## RESULTS

### Shuttling of HST between nucleus and cytoplasm can be uncoupled from its role in the miRNA pathway

In *hst* mutants, some miRNAs accumulate to a lower level, but the nucleus/cytoplasm ratio of miRNAs is not altered in *hst* mutants as demonstrated by cell fractioning [(Park et al., 2005), Figure 1A, Supplemental Figure 1A)]. Most karyopherins-like cargo proteins, such as EXP5, conduct nuclear transport in cooperation with the small GTPase RAN (Merkle, 2011). Exportins associated with RAN-GTP bind cargo molecules in the nucleus, which are released in the cytoplasm after GTP hydrolyzation. HST is not an exception and also interacts with the GTPase RAN1 (Bollman et al., 2003). We therefore, asked whether RAN1 is required for miRNA accumulation and/or for partitioning miRNAs between nucleus and cytoplasm. RNA blots revealed that different from *hst-15*, *ran1* mutants did not show any reduction in the miRNA pool (Figure 1B, Supplemental Figure 1B). The nuclear/cytoplasmic ratio of miRNAs in *ran1* also appeared to be unchanged (Figure 1C, Supplemental Figure 1C). In *A. thaliana*, *RAN1* (AT5G20010) has two close homologs, *RAN2* (AT5G20020) and *RAN3* (AT5G55190). Therefore, we asked whether redundancy was masking any involvement of RAN1 in miRNA biogenesis. We were able to obtain doubly homozygous *ran1 ran3* and *ran2 ran3*, but not *ran1 ran2* double mutants, as *RAN1* and *RAN2* genes are tandem duplicates and very closely linked in the genome (Supplemental Figure 1D). All *ran* single or double mutants were normal in appearance under standard growing conditions (Supplemental Figure 1E). Similar to single mutants, both total miRNA levels and their nuclear/cytoplasmic partition were comparable to the controls in the *ran2, ran3*, *ran1 ran3,* and *ran2 ran3* mutants (Figure 1B and 1C, Supplemental Figure 1B, 1C, 1G, and 1F). *ago1* mutants, recently described to be defective in miRNA export from the nucleus (Bologna et al., 2018), were used as controls of impaired exporting (Figure 1C, Supplemental Figure 1C and 1F).

As we could not exclude redundancy among RAN proteins due to the lack of triple *ran1 ran2 ran3* mutants, we also took a parallel approach. HST was shown to interact with RAN1, and potentially with other redundant GTPase, through its N-terminal domain (Bollman et al., 2003). Thus, we created a

truncated version of the protein lacking the first 107 first amino acids [GFP:HST$^{\Delta N}$, (Bollman et al., 2003)] aiming to eliminate HST interaction with any RAN-like homolog. We used this construct, or a transgene expressing full-length HST, to transform *hst-15* mutants and once again evaluate total miRNA abundance and its subcellular partition. The total amount of some miRNAs, but not the nuclear/cytoplasmic partition ratio, appeared altered in the *hst-15* mutants complemented with the GFP:HST$^{\Delta N}$ construct (Figure 1C-E). This suggests that this portion of the protein, as full length HST, is necessary for miRNA accumulation but dispensable for miRNA nuclear/cytoplasmic movement. Mammalian EXP5 has recently been shown to be required for miRNA processing in a RAN GTPase-independent manner (Wang et al., 2020). By analogy, our data suggested that a potential exporting function of HST, if any, and its interaction with RAN1 are dispensable for miRNA movement from nuclei to cytoplasm, potentially allowing us to uncouple a presumed function of HST as exportin from its role in the miRNA pathway.

**RAN1 and IMPA-2 modulate HST nuclear/cytoplasm shuttling but not miRNA export**

To further aimed to understand the role of the N-terminal region of HST, and the influence of RAN1, in regulating the cellular distribution of HST and miRNA production. We transformed Col-0, *hst-15*, *ran1, ran2,* and *ran3* mutants with a GFP tagged version of HST, or of HST$^{\Delta N}$, and evaluated the protein localization by confocal microscopy. Both the full-length HST and to HST$^{\Delta N}$ constructs produced proteins of the expected size as detected by western blot (Supplemental Figure 2A). However, only the full-length GFP:HST fusion reverted *hst-15* morphological defects (Supplemental Figure 2B). The lack of phenotypic complementation by HST$^{\Delta N}$ coincided with the failure of this protein to restore miRNA production in *hst-15* (Figure 1D and 1E). In agreement with previous reports, we found HST predominantly located in the nucleus, with low levels detected in the cytoplasm [(Bollman et al., 2003) Figures 2A-C]. In *ran1* mutants, but not in *ran2* or *ran3* mutants, we observed a significant reduction in the cytoplasmic faction of GFP-HST, compatible with the proposed role of RAN1 in HST shuttling (Figure 2B and 2C, Supplemental Figure 2C). *ran1 ran3* , but not *ran2 ran3,* mutants also had a reduced cytoplasmic pool of GFP-HST

(Figure 2B and 2C). This result indicates that mainly RAN1 is required for the export of HST from the nucleus to the cytoplasm.

The fact that we detected HST, albeit at very low levels, in the cytoplasm of *ran1* and *ran1 ran3* mutants suggested a certain degree of redundancy among *RAN* homologs. Thus, we evaluated the localization of GFP:HST$^{\Delta N}$ that does not interact with RAN proteins. Unexpectedly, GFP:HST$^{\Delta N}$ showed a shift of the nucleus/cytoplasm fluorescent ratio toward the cytoplasm and a reduction of fluorescent signal in the nucleus, while an HST variant with a deletion of the C-terminal end (GFP:HST$^{\Delta C}$), used as a control, behaved similarly as the full-length protein (Figure 2B and 2C). We co-transformed the truncated versions of HST fused to GFP with the wild-type version of the protein fused to mCherry and compared fluorescence ratios confirming nuclear exclusion of HST$^{\Delta N}$ (Figure 2D). The nuclear exclusion of GFP:HST$^{\Delta N}$ became more evident when we extended the N-terminal deletion from amino acid 107 to 322 (GFP:HST$^{\Delta N322}$) (Figure 2E and 2F). Such stronger effect in HST$^{\Delta N322}$ is probably the consequence of the removal in this construct, but not in HST$^{\Delta N}$, of one of the two predicted NLS of HST(Figure 2E). As the N-terminal region of HST is supposed to interact with RAN1, which in turn is required for shuttling of karyopherin-like cargo proteins to the cytoplasm, the observed cellular distribution of GFP:HST$^{\Delta N}$ was unexpected, seemingly contradicting the previous observation that *ran1* mutants have less cytoplasmic HST (Figure 2B and 2C). The fact that HST is preferentially located in the nucleus when RAN1 is absent, but in the cytoplasm when the N-terminal RAN-interacting region of HST is removed, suggested that this portion of the protein also interact potentially with other factors controlling the shuttling of neo-translated HST into the nucleus.

Aiming to identify which factor could interact with the N-terminal region of HST and shuttle the protein from the cytoplasm to the nucleus, we immunoprecipitated GFP:HST and GFP:HST$^{\Delta N}$ and searched for associated proteins by mass spectrometry. Among the proteins associated with HST, we detected, as expected, RAN1/2/3 (Supplemental Table 1), validating the specificity of our experiments. Among proteins interacting with the full-length version of HST, but not with HST$^{\Delta N}$, we detected the alpha importin IMPA-2 (encoded by *AT4G16143*), a homolog of the human nuclear protein importines

KPNA1 and KPNA2. BiFC assays with HST:N-mCitrine or HST$^{\Delta N}$:N-mCitrine and IMPA-2:C-mCitrine confirmed that only full-length HST interacts with IMPA-2 (Figure 3A). HST-IMPA-2 interaction appeared to occur in both the nucleus and cytoplasm, which is compatible with the known shuttling of exportins and importins. Since IMPA-2 is an α-importin, its interaction with the N-terminal domain of HST may mediate HST shuttling from the cytoplasm to the nucleus. Such inference may explain our observation that GFP:HST$^{\Delta N}$ preferentially accumulated in the cytoplasm, as this HST variant may not be transported to the nucleus in the first place (Figures 2C-F). To test this possibility, we transformed *impa-2* mutants (SALK_099707) and wild-type plants with GFP:HST and GFP:HST$^{\Delta N}$ and quantified nuclear/cytoplasmic distribution of HST by confocal microscopy. Consistently with a role of IMPA-2 transporting HST to the nucleus, we observed a drastic reduction in the number of nuclei containing detectable GFP signal in *impa-2* mutants, similar to GFP:HST$^{\Delta N}$ in wild type (Figure 3B and 3C). Nuclei with GFP:HST$^{\Delta N}$ signal were even rarer in the *impa-2* mutant background (Figure 3C). Finally, the few *impa-2* cells with a visible signal in the nucleus presented a significant reduction of the GFP nucleus/cytoplasm intensity ratio both for the full-length HST and HST$^{\Delta N}$ proteins (Figure 3D, Supplemental Figure 2C).

As IMPA-2 appeared to alter the subcellular distribution of HST, we assayed total and nuclear/cytoplasmic accumulation of miRNAs in *impa-2* mutants by RNA blot. We did not detect any change in the nucleus/cytoplasm miRNAs ratio in the mutant (Figure 3F), again supporting our conclusion that HST is not involved in miRNA export from the nucleus or at least is not acting as the main source of miRNA exporting. However, the overall accumulation of miRNAs in *impa-2* appeared reduced as in *hst-15* mutants (Figure 3E and 3F). This observation is compatible with the known role of HST in miRNA biogenesis, as *impa-2* mutants presented reduced amounts of nuclear HST, which is the fraction of HST presumably acting in miRNA biogenesis.

**HST associates with mature miRNAs but is not directly involved in pri-miRNA processing**

To evaluate the genome-wide effects of *hst* on miRNA biogenesis, we profiled miRNAs by small RNA sequencing in *hst-15* and *hst-15* plants

transformed with *GFP:HST* and *GFP:HST*$^{\Delta N}$. As expected, we observed a moderate decrease in levels of several miRNAs and miRNA*s in *hst-15* mutants (Figure 4A and 4B, Supplemental Figure 3A, Supplemental Table 2). The full-length version of HST, but not the one lacking the N-terminal portion, was able to restore miRNA accumulation to wild-type levels (Figure 4A and 4B, Supplemental Figure 3A). This analysis agreed with our miRNA measurements using sRNA blots and RT-qPCR (Figure 1D and 1E). Although, not all miRNAs appeared repressed in *hst-15* and some, such as miR157, may even increase in the *GFP:HST*$^{\Delta N}$ plants (Figure 1D and 4A, Supplemental Table 2). A comparison of small RNA sequencing data revealed *hst-15* down-regulated miRNAs largely correlated with those repressed in processing mutants, such as *hyl1-2* and *se-3*, but to a lesser extent with mutants in CARP9, a protein acting in post-processing steps of the pathway (Figure 4C). As expected, the reduction in miRNA accumulation in *hst-15* translated into deficient gene silencing as miRNA-targeted mRNAs overaccumulated in *hst-15* mutants (Figure 4D, Supplemental Table 3).

To assay the effects of *hst* on pri-miRNA accumulation and silencing of miRNA targets, we developed a cost-efficient mRNA-seq protocol that supports multiplexing of up to 576 samples through Nextera barcoded PCR primers (Supplemental Material and Methods). The on-bead reactions reduce bench-work time and increase the efficiency of the reactions. The experiment revealed an over-accumulation of unprocessed pri-miRNAs in *hst-15* mutant (Figure 4D). Normal levels of pri-miRNAs were detected in *hst-15* mutants expressing full-length HST, but not GFP:HST$^{\Delta N}$, as measured by RT-qPCR (Supplemental Figure 3B). The over-accumulation of pri-miRNAs in *hst-15* is probably the consequence of impaired processing as reported for other miRNA mutants (Kurihara et al., 2006; Lobbes et al., 2006). However, enhanced transcription of *MIRNA* genes, either as a feedback-loop caused by the reduced mature miRNAs or a direct transcriptional effect of HST, cannot be discarded as a possibility. As a matter of fact, when we transformed Col-0 and *hst-15* protoplasts with a MIR171A$_{promoter}$:GUS construct (Manavella et al., 2013) we observed higher levels of the reporter gene in the mutant background indicating enhanced transcription (Supplemental Figure 3C).

Pri-miRNA profile in *hst-15* showed the highest correlation with *dcl1-9* mutants when mRNA-seq data sets were compared (Figure 4E). Thus, another possibility is that HST directly affects miRNA processing as EXP5 does in animals (Wang et al., 2020). To evaluate this possibility, we performed *in vitro* processing assays using protein extracts from *hst-15* mutants. To this end, we transcribed *in vitro* an artificial miRNA precursor targeting the reporter gene LUCIFERASE [pri-amiRLUC, (Manavella et al., 2012)] and incubated it with crude protein extract from wild-type plants and *hst-15* mutants, as well as *dcl1-100* mutants, as a positive control for plants with impaired miRNA processing. We quantified pri-miRNA processing efficiency by RT-qPCR of mature amiRLUC. As expected, we observed pri-miRNA processing with protein extracts from wild-type plants and a clear failure of processing with *dcl1-100* protein extracts (Figure 4F). Protein extracted from *hst-15* mutant plants showed pri-miRNA processing activity comparable to that of wild-type plants (Figure 4F). This result indicated that despite HST requirement for miRNA accumulation, HST is not required for the dicing activity of DCL1. RNA immunoprecipitation assays (RIP) showed that HST does not interact with pri-miRNAs *in vivo*, which would be expected if HST participated in miRNA processing (Figure 4G). We performed HYL1 RIP as a positive control of pri-miRNA interaction with a protein (Figure 4G).

The lack of a direct effect of HST on miRNA processing, but impaired miRNA accumulation in the mutants, could reflect an indirect role of HST regulating other miRNA-biogenesis factors. To test this possibility, we quantified mRNA and protein levels of the major miRNA biogenesis factors *AGO1*, *DCL1*, *SE*, and *HYL1* by mRNA-seq. We detected more *AGO1* transcripts, probably as a consequence of the low levels of miRNA168 (Supplemental Table 2 and 3, Figure 4H). However, such a difference was not evident at the protein level (Figure 4I). No differences in mRNA or protein levels were observed for *DCL1*, *SE*, and *HYL1* (Supplemental Table 3, Figure 4H and 4I). No other miRNA biogenesis-related gene appeared particularly de-regulated in *hst15* mutant, based on the mRNA-seq data (Supplemental Table 3). This suggested that HST does not affect miRNA biogenesis by modulating the levels of other proteins from the core miRNA-biogenesis complex. Despite not detecting pri-miRNAs associated with HST, the RIP assays showed that GFP:HST, but not

GFP:HST$^{\Delta N}$, was able to interact with mature miRNAs (Figure 4J). To exclude a bias caused by differential localization of each construct we equalized immunoprecipitated nuclear proteins using saturating IP conditions. For this, a high amount of nuclear proteins were incubated with half the amount of beads recommended by manufacturers to ensure beads saturation and equal precipitation of GFP:HST and GFP:HST$^{\Delta N}$ between samples (Supplemental Figure 2A). Since we used cross-linked samples for the RIP assays, the HST-miRNA interaction does not necessarily imply a direct association between the molecules. Thus HST-miRNA interaction, which also appeared to be dependent on the N-terminal region of HST, might also result from HST interaction with a miRNA-associated factor.

**HST stabilizes DCL1 interaction with the mediator complex**

Our data indicated that HST function in the miRNA pathway is independent from any exportin function and that HST does not act in miRNA processing itself. On the other hand, our experiments were compatible with a scenario in which HST acts as a scaffold protein for miRNA biogenesis factors and in which HST is required for the correct assembly of the pri-miRNA-processing complex. To test this hypothesis, we first performed BiFC assays to find out whether HST interacts with known proteins in miRNA biogenesis. BiFC experiments revealed that HST:N-mCitrine interacted with DCL1:C-mCitrine, HYL1:C-mCitrine, SE:C-mCitrine and CPL1:C-mCitrine (Figure 5A, Supplemental Figure 4A). It is important to note that BiFC assays do not necessarily indicate direct protein-protein interaction but rather that proteins belong to the same protein complex. Yeast two-hybrid (Y2H) assays confirmed a direct interaction of HST with DCL1, but failed to support direct interactions of HST with HYL1, SE, CPL1, and HEN1 (Figure 5B).

Because DCL1 interacts with mature miRNAs (Baranauske et al., 2015), we wondered whether DCL1 interaction with HST could explain the HST-associated miRNAs detected in our RIP assays. Since HST$^{\Delta N}$ did not associate with miRNAs it could be expected, if our hypothesis is correct, that this truncated version of HST also fails to interact with DCL1. In agreement with this hypothesis, Y2H and BiFC assays revealed that different from the full-length protein, HST$^{\Delta N}$:N-mCitrine did not interact with DCL1:C-mCitrine (Figure 5B and

5C, Supplemental Figure 4A). We observed GFP signal when HST$^{\Delta N}$:N-mCitrine was assayed with HYL1:C-mCitrine, SE:C-mCitrine and CPL1:C-mCitrine which may indicate that the small portion of HST$^{\Delta N}$ entering the nucleus is still able to be recruited to the processing complex (Figure 5C, Supplemental Figure 4A). These results suggested that DCL1-HST interaction depends on the N-terminal domain of HST, but that this region is dispensable for HST association with the processing complex, implying that HST can associate with the processing machinery independently of its interaction with DCL1. The failure of GFP:HST$^{\Delta N}$ to revert *hst-15* phenotypes and miRNA production (Figure 1D) suggested that DCL1-HST interaction, but not its association with the HYL1-, SE- or CPL1-containing complex, is required for HST activity in the miRNA pathway.

Aiming to understand how the HST-DCL1 interplay may affect miRNAs production, we returned to our mass spectrometry assays data searching for potential HST partners. A GO molecular function analysis with Panther (Mi et al., 2019) of HST interacting proteins (Supplemental Table 1) revealed several members of the poly(U) RNA binding- and mRNA binding- proteins (Supplemental Table 4). Among them, we found four subunits of Mediator37 (MED37-C/D/E/F), four transcription factors and enhancers of gene transcription, and eight RNA binding proteins and RNA helicases (Supplemental Table 1). In particular, the mass spectrometry data indicated that MED37 associates with both the full-length HST and HST$^{\Delta N}$ mutant (Supplemental Table 1).

Because the mediator complex is required for pri-miRNA transcription and miRNA accumulation (Kim et al., 2011), we performed BiFC assays between HST/HST$^{\Delta N}$:N-mCitrine and MED37-D/E/F:C-mCitrine. Confirming the mass spectrometry results, both full-length HST and HST$^{\Delta N}$ interacted with MED37-D and MED37-E but not with MED37-F (Supplemental Figure 4B). HST-MED37D interaction was further validated by Y2H assays (Supplemental Figure 4C). This interaction of HST with the mediator complex, especially with HST$^{\Delta N}$, suggested that HST could be recruited to *MIRNA* genes even in the absence of DCL1 interaction. This observation could also explain why HST$^{\Delta N}$ gives a positive BiFC signal with HYL1, SE and, CPL1, as they also associate with *MIRNAs* loci potentially positioning these proteins nearby (Achkar et al.,

2016; Koiwa et al., 2004; Wang et al., 2019). Unlike *MED17*, *MED18*, and *MED20* which mutations cause morphological defects (Kim et al., 2011), neither MED37-D (SALK_111603.53.70), MED37-E (SALK_135531.41.60), nor MED37-F (SALK_073202.46.15) single mutants have any apparent phenotype. This lack of phenotype is likely caused by gene redundancy as six genes encode MED37 homologues in Arabidopsis (Supplemental Figure 4D and 4E). Among them, five appeared potentially interacting with HASTY, MED37-C, -D, -E, -F/A (Supplemental Table 1, Supplemental Figure 4B and 4C).

Since the N-terminal domain of HST interacts with DCL1, and a different region with MED37, it is possible that the formation of a complex between these three proteins promote the recruitment of DCL1 to *MIRNA* loci. To test this hypothesis, we first evaluated whether DCL1 and MED37-D/E interact by BiFC assay in *N. benthamiana* leaves. The experiment revealed a barely detectable interaction signal between DCL1 and MED37 (Figure 5D). However, when we repeated the assay in plants over-expressing HST (TriFC assay), reconstitution of fluorescence was clearly visible in the cell nucleus, suggesting that HST acts as a scaffold stabilizing a complex containing DCL1 and the mediator complex (Figure 5D). Moreover, nuclear speckles, proposed sites of miRNA processing (Achkar et al., 2016), were apparent in this triple interaction assay (Figure 5D). We further confirmed this result by a yeast-three-hybrid (Y3H) assay, where we only detected yeast growth in a selective medium when cells expressed HST together with DCL1 and MED37D (Supplemental Figure 4F).

The function of DCL1 in the miRNA pathway is to catalyze the dicing of miRNA precursors to release the mature miRNA duplexes. DCL1 activity is not impaired in *hst-15*, suggesting that HST does not directly modulate DCL1 activity or pri-miRNA processing. DCL1 can interact with *MIRNA* loci, probably by its recruitment to nascent pri-miRNAs (Fang et al., 2015). Having found that HST stabilizes the DCL1-MED37 interaction, we hypothesized that HST could participate or stabilize the interaction of DCL1 to *MIRNA* genes instead of modulating DCL1 enzymatic activity. To test this hypothesis, we first evaluated by ChIP-qPCR whether MED37E and D associate with MIRNA loci, as it is the case for MED17, 18 and 20 (Kim et al., 2011). The experiment revealed that both MED37 proteins interact with MIR159A, MIR166A, MIR167A and MIR167C loci, while only MED37E interacts with MIR165A locus, and none of them

appeared significantly enriched in the MIR164A locus (Figure 5E). We then confirmed using ChIP-qPCR of GFP tagged HST that this protein also associates with MIRNA loci in cross-linked samples (Figure 5F). Interestingly, when we tested HST interaction with MED20, known to regulate miRNA genes (Kim et al., 2011), we obtained a positive interaction by BiFC but, contrary to MED37, a negative interaction by Y2H (Supplemental Figure 4C and 4G). This result suggests that HST forms a complex with MED20, probably through MED37, but do not directly interact with this subunit of the complex. Along with this result, we found MED37D in the same complex as MED20 by BiFC but failed to detect a direct interaction by Y2H (Supplemental Figure 4C and 4G). As MED20 is, together with MED17 and 18, a core component of the head module of the mediator complex (Dolan and Chapple, 2017), it is likely that the MED37-HST-DCL1 interaction occurs through a different module of the complex. Finally, we performed DCL1-ChIP-qPCR to measure DCL1 occupancy at *MIRNA* genes in wild-type and *hst-15* plants. DCL1 occupancy at *MIRNA* genes was detected in wild type, as previously reported, but little or no signal was detected in *hst-15* (Figure 5G). These results suggested that DCL1 interaction with *MIRNA* loci is promoted or stabilized by HST, probably modulating co-transcriptional assembly of the processing complex to nascent pri-miRNAs in a Mediator dependent manner. Along with this idea, the association of pri-miRNAs to HYL1, a well-known DCL1 interacting protein, also appeared reduced in *hst-15* mutants as revealed by RIP-qPCR experiments (Figure 5H).

## Discussion

For many years now, the transport of plant miRNAs from the nucleus to the cytoplasm was often attributed to HST even when this function was not supported by experimental data (Bollman et al., 2003; Guo et al., 2014; Merkle, 2011; Park et al., 2005). *hst* mutants present low levels of some miRNAs, which seem to cause most of the characteristic phenotypes of these plants (Allen et al., 2013; Bollman et al., 2003; Fang et al., 2015; Peragine et al., 2004; Telfer and Poethig, 1998; Ueno et al., 2007; Zhang et al., 2017a; Zhu et al., 2019). Nevertheless, our data shows that even when some miRNAs present a moderate reduction in accumulation, many remain at homeostatic levels

suggesting that HST may act on a specific subset of miRNAs (Supplemental Table 2, Figure 4A and 4B).

In this study, we found that RAN1 and IMPA-2 modulate HST shuttling between the nucleus and the cytoplasm. In agreement with previous reports (Bologna et al., 2018; Park et al., 2005; Zhang et al., 2017b; Zhu et al., 2019), we did not observe any change in nuclear/cytoplasm fractions of miRNAs in plants impaired in HST, RAN, or IMPA-2 activity. HST is a β-like nuclear-cytoplasmic shuttling protein similar to the human KPNB1 that shuttles proteins to the nucleus also by interacting with IMPA-2 and RAN proteins (Luo et al., 2013). Thus, HST could in principle control the shuttling of miRNA biogenesis factors, as is the case of the RAN1-interacting karyopherin KETCH1 that allows the nuclear import of HYL1 (Zhang et al., 2017b). However, HST did not appear to influence the nuclear/cytoplasmic distribution of several tested factors (Zhang et al., 2017b).

HST interacts with RAN1 through its N-terminal domain (Bollman et al., 2003), a domain that we also found to be required for HST function in miRNA biogenesis. This domain also interacts with IMPA-2, which in turn aids the translocation of HST to the nucleus. Given that both IMPA-2 and RAN1 appeared to interact with the same region of the protein, it is plausible that the association of either protein with HST is mutually exclusive.

We have demonstrated that HST does not interact with pri-miRNAs, nor affect DCL1 activity, indicating that its activity is not directly associated with pri-miRNA processing nor in the miRNA export. Instead, full-length HST, but not a version missing the N-terminal domain, interacts with mature miRNAs. In animals, the N- and C-terminal domains of EXP5 interact with each other, leading to the formation of a closed ring-like structure that fail to bind pre-miRNAs (Wang et al., 2011b; Yamazawa et al., 2018). Upon association with RAN1, EXP5 adopts a U-like structure, that bind pre-miRNAs (Yamazawa et al., 2018). The inability of $HST^{\Delta N}$ to interact with RAN1 may stabilize a ring-like structure blocking the miRNAs binding. Another possibility is that the N-terminal region allows the interaction with a partner protein loaded with miRNAs, perhaps DCL1. In any case, the apparent ability of HST to interact, either directly or indirectly, with mature miRNAs is intriguing, particularly given that the levels of many miRNAs are not, or only moderately, affected in hst mutant. This

could suggest that HST only acts upon a subfraction of these molecules, with this proposed subfraction possibly varying in extent from one miRNA to another (Figure 4). A recently discovered pool of AGO1-unloaded miRNAs might represent this subfraction of HST-interacting species (Dalmadi *et al.,* 2019) because they would be expected to evade nuclear AGO1 loading and subsequent export of miRISC through the TREX-2 and XPO1-dependent pathway. Whether this subfraction of miRNAs is defined early during the HST-DCL1 interaction reported here also remains to be addressed. Whether this small subfraction of miRNAs is exported by HST to have an specific function in the cytoplasm also remains as an open question.

In summary, we demonstrated that HST is not required for DCL1 RNase III activity or aas a main source of miRNA export but rather enhances the initial recruitment of DCL1 to *MIRNA* loci. HST can directly interact with DCL1 through its N-terminal domain, potentially explaining why we detected mature miRNAs associated with HST. Recruitment of DCL1 to *MIRNA* genes is impaired in *hst* mutants, apparently because a MED37-DCL1 complex is destabilized. Our data allows us to propose a model where HST modulates miRNA biogenesis by recruiting DCL1 to nascent pri-miRNAs (Figure 6). At this point, HST may interact with MED at *MIRNA* genes preceding DCL1 recruitment to the loci. This may allow, or stabilize, the assembly of the processing complex early during pri-miRNA transcription. An important question for the future is how HST itself is recruited to *MIRNA* loci and whether this karyopherin protein has any function transporting cargos between the nucleus and the cytoplasm. Whether the miRNAs produced by a HST-DCL1-mediated pathway are early programed to have specific functions in the cytoplasm is also a possibility worth exploring.

## Material and methods

### Plant material and growth condition

Seeds of *Arabidopsis thaliana* accession Columbia (Col-0, CS22681), *hst-15* (SALK_079290), *ran1-1* (SALK_138680)*, ran1-2* (SALK_067649), *ran2* (SALK_123620)*, ran3* (SALK_078740), *ago1-25*, *ago1-27* and *impa-2* (SALK_099707) were used in this study. *ran1-1/ran3* and *ran2/ran3* double mutants were generated in this study. *A. thaliana* and *N. benthamiana* seeds

were sterilized with 10 % (vol/vol) aqueous bleach and 0.5 % SDS and stratified for 2-3 days at 4 °C.

**Transgenes**

Plasmid used to transform *Nicotiana benthamiana* or *A. thaliana* are listed in Supplemental Table 5. DCL1:C/N-mCitrine, CPL1:C-mCitrine, SE:C-mCitrine, and HYL1:C-mCitrine were previously reported (Manavella et al., 2012). Primers used for cloning are listed in Supplemental Table 6. In all cases, genes were amplified using Phusion polymerase (Thermo Fisher), cloned in pEntr/D-TOPO (Thermo Fisher), and recombined with LR-clonase (Thermo Fisher) into Gateway compatible pGreen destination vectors. *Agrobacterium tumefaciens* infiltration of 2-week old *N. benthamiana* leaves was performed for sub-cellular localization assays following a standard protocol (de Felippes and Weigel, 2010). Briefly, *A. tumefaciens* (GV3101-pMP90) harboring the gene of interest on a binary plasmid was grown on selective Luria-broth (LB) medium. Bacteria were pelleted and resuspended in infiltration medium (10 mM MgCl2, 10 mM MES pH 5.7, 150 µM acetosyringone). After four hours of incubation at room temperature (21-23°C) and gentle agitation, plants were infiltrated with a suspension at an optical density of 0.5 at 600 nm. After three days, samples were analyzed on a TCS SP8 confocal microscope (Leica, Solms, Germany). *A. thaliana* transgenic plants were obtained by floral dip (Zhang et al., 2006). Protoplast preparation and transformation was performed as previously described (Wu et al., 2009).

**RNA analysis**

Total RNA was extracted using TRIzol reagent (Thermo Fisher Scientific). RNA blots were performed as previously described (Tomassi et al., 2017). Briefly, 2 µg of total RNA were resolved in 17% (v/v) polyacrylamide gels under denaturing conditions (7 M urea) and then transferred to HyBond-N+ charged nylon membranes (Amersham) by semidry electroblotting. RNA was covalently fixed to membranes in an UV Crosslinker. Membranes were hybridized overnight with DNA oligonucleotide probes labeled with DIG (Alpha DNA Company). Signal was detected using CSPD ready-to-use solution, by exposure to Amersham hyperfilm ECL (GE Healthcare Life Sciences). For

quantitative RT-qPCR, 1 µg of total RNA was treated with DNase I (Thermo Fisher Scientific) and cDNA was produced with RevertAid RT Reverse Transcription Kit (Thermo Fisher Scientific). Quantitative qPCRs were performed on three biological replicates (5 seedlings each), Actin 2/8 (At3g18780/At1g49240) was used as reference gene. Fold change was calculated by the $2^{-\Delta\Delta Ct}$ method. Error shown corresponds to SEM. Statistical differences ($p<0.05$ or $p<0.01$) were calculated by ANOVA followed by Tukey's multiple comparison test, or by two tailed unpaired *t*-test analysis and corrected with FDR for multiple pair comparisons.

**Nuclear-cytoplasmic fractionation**

Nuclear-cytoplasmic fraction were obtained as described by Wang et al. (Wang et al., 2011a) with minor modifications. Briefly, 3 g of two-week old seedlings grown on MS agar plates were harvest and ground in 6 mL of lysis buffer (20 mM Tris-HCl, pH 7.5, 20 mM KCl, 2 mM EDTA, 2.5 mM MgCl2, 25 % glycerol, 250 mM sucrose, and 5 mM DTT). The suspension was filtered through a double layer of Miracloth (Calbiochem) and centrifuged at 1,500 g for 10 min. The supernatant was centrifuged at 10,000 g for 10 min at 4°C and collected as cytoplasmic fraction. The pellet was washed four times with 10 mL of nuclear resuspension buffer NRBT (20 mM Tris-HCl, pH 7.4, 25 % glycerol, 2.5 mM $MgCl_2$, and 0.2 % Triton X-100) and then resuspended with 500 mL of NRB2 (20 mM Tris-HCl, pH 7.5, 0.25 M sucrose, 10 mM $MgCl_2$, 0.5 % Triton X-100, and 5 mM b-mercaptoethanol). It was carefully overlaid on top of 700 mL NRB3 (20 mM Tris-HCl, pH 7.5, 1.7 M sucrose, 10 mM $MgCl_2$, 0.5 % Triton X-100, and 5 mM β-mercaptoethanol), and centrifuged at 16,000 g for 10 min at 4°C. The nuclear pellet was directly resuspended in TRIzol reagent for RNA extraction.

**RNA immunoprecipitation**

For RNA immunoprecipitation experiments, 2 grams of 10-day-old seedlings grown on MS agar plates were collected after formaldehyde crosslinking. Anti-HYL1 (Agrisera) or anti-GFP (Abcam) and SureBeads Protein-A magnetic bead (Bio-Rad) were used to immunoprecipitate HYL1-RNA or GFP:HST/$HST^{\Delta N}$-RNA complexes. Half of the amounts of beads suggested

by manufacturer were used in GFP:HST/HST$^{\Delta N}$ RIP assay, in order to saturate the beads and evaluate equal levels of proteins obtained from purified nuclei. Negative control was performed by immunoprecipitating unspecific proteins with anti IgG (Abcam). Reverse crosslinking was performed with proteinase K (Qiagen). After discarding the beads, the supernatant was used for RNA extraction using TRIzol reagent (Thermo Fisher Scientific) (Francisco-Mangilet et al., 2015).

**Chromatin immunoprecipitation**

Chromatin immunoprecipitation (ChIP) assays were adapted from Lucero et al (Lucero et al., 2017). Five grams of seedling growth in MS agar media were crosslinked with formaldehyde. Enriched nuclei were sonicated in a Bioruptor Pico water bath (Diagenode; 30 s on/30 s off pulses at high intensity for 10 cycles, using Bioruptor microtubes). Samples were incubated with Anti-DCL1 (Agrisera) or Anti-IgG (Abcam; as negative control) and immunoprecipitated with SureBeads Protein-A magnetic bead (Bio-Rad) for 12 h at 4 °C. Reverse crosslinking was performed with proteinase K (Qiagen). Immunoprecipitated DNA was recovered using phenol:chloroform:isoamyl alcohol mix (25:24:1), ethanol precipitation, and analyzed by qPCR. Untreated sonicated chromatin was processed in parallel and considered the input sample. Statistical differences between samples ($p < 0.01$) were determined ANOVA using Tukey's multiple comparison test.

**Protein blot**

Proteins were extracted from 100 mg ground tissue with 100 µl extraction buffer (50 mM Tris [pH 7.5], 150 mM NaCl, 1 mM EDTA, 10 % [v/v] Glycerol, 1 mM DTT and one tablet Complete Protease Inhibitor Cocktail [Roche] per 10 ml of prepared buffer). SDS-PAGE (8%) was run and transferred to PVDF membrane (Amersham). Anti-SE, -HYL1, -AGO1, -DCL1 and -ACTIN 8 (Agrisera) or anti-GFP (Abcam) were used to detect proteins. The intensity of the bands was measured with ImageJ and normalized to ACTIN 8.

**Protein-protein interaction**

For BiFC assays, *N. benthamiana* plants were transformed as previously described and fluorescence intensity in each sample was detected by confocal microscopy. For TriFC assays, GFP signal was detected in plants transformed with 35S:MED-37:C-mCitrine and 35S:DCL1:N-mCitrine (Supplemental Table 5), in the presence or absence of 35S:HA:HST. Samples without 35S:HA:HST were co-transformed with an empty vector instead. Quantification of the GFP signal was with ImageJ, and significant differences ($p<0.01$) were detected by two-tailed, unpaired, *t*-test analysis. Yeast two-hybrid assays were performed with the ProQuest Two-Hybrid System (Thermo Fisher Scientific). 10 mM 3-amino-1,2,4-triazole (3-AT) was added to the selective media to reduce auto-activation. For co-immunoprecipitation followed by LC-MS/MS, 5 g of seedlings from two independent transgenic lines expressing GFP:HST, GFP:HST$^{\Delta N}$ or GFP (as negative control) were harvested and ground in extraction buffer (50 mM HEPES, 150 mM KCl, 1 mM EDTA, 0.5 % Triton X-100, 1 mM DTT, and one complete EDTA-free PI tablet Roche Cocktail [Roche] per 10 ml of prepared buffer). After centrifugation at max speed, immunoprecipitation was performed using GFP-Trap (Chromotek) following the manufacturer instruction and using the extraction buffer as washing buffer. The last wash was performed with the same buffer without Triton X-100. Proteins from beads were then eluted with 0.1 M Glycine pH 2.2, and then pH neutralized with 0.15 µl of 1 M Tris pH 8.3. For LC-MS/MS, SDS-PAGE (short run) Tryptic in gel digestion was performed, LC-MS/MS analysis was done on a Proxeon Easy-nLC 1200 coupled to a QExactive HF mass spectrometer; method: 60 min, Top12 HCD. The data was processed employing MaxQuant software suite v.1.5.2.28 (Cox and Mann, 2008; Cox et al., 2011). Using the Andromeda search engine the spectra were searched against the Uniprot *A. thaliana* database. The processing of the raw data was done with 1 % FDR (False Discovery Rate). Interacting proteins were called only when a difference of two or more peptides were found between GFP:HST, GFP:HST$^{\Delta N}$ and GFP samples. This filter included proteins where iBAQ is equal to zero in control plants or a difference higher than 100,000 between samples and control.

### *In vitro* DCL1 activity

*In vitro* DCL1 activity measurements in Col-0, *hst*-15, and *dcl1-100* were performed as previously reported (Qi et al., 2005) with modifications. Artificial pri-miRLUC (*pri-amiRLUC*) (Manavella et al., 2012) was *in vitro* transcribed by T7 RNA polymerase (Promega). The transcribed pri-amiRLUC was used as substrate for *in vitro* processing by analyzing the accumulation of resulting mature amiRLUC by RT-qPCR. pri-amiRLUC (1 µg) and 15 µl of protein extracts from inflorescence (1 mg/ml) were mixed with 5x reaction buffer (0.5 M NaCl, 10 mM ATP, 2 mM GTP, 6 mM $MgCl_2$, 20 mM phosphoenolpyruvate, 5 U Pyruvate kinase, 2 U RNasin [Promega]) in final reaction volume 20 µl. The reaction was carried for 3 hr at 25 C°, and stopped by adding TRIzol. A first RNA precipitation was performed with LiCl 2.5 mM, and supernatant was then precipitated with Isopropanol supplemented with 1 µl glycogen. RT-qPCR was performed with specific primers listed in Supplemental Table 6.

**sRNA-seq and mRNA-seq**

With 1 µg of total RNA as input, small RNA libraries were prepared with the TruSeq small RNA library prep kit (Illumina) as described in the TruSeq RNA sample prep V2 guide (Illumina). Small RNA libraries size selections were performed using the BluePippin System (SAGE Science). Illumina sequencing was performed with a HiSeq3000 apparatus. Small RNA reads were first cut to remove 3´ adapters using cutadapt [version 1.9.1; (Martin, 2011)] and their quality checked using FastQC (version 0.11.4, https://www.bioinformatics.babraham.ac.uk/projects/fastqc/) and MultiQC (Ewels et al., 2016). They were then mapped with bowtie [version 1.1.2; (Langmead et al., 2009)] to *A. thaliana* rRNA, tRNA, snoRNA and snRNA from RFAM [version 14.1, (Kalvari et al., 2018)]. Unmapped reads were then mapped, also with bowtie, to the following references: the databases for hairpin and mature miRNAs for *A. thaliana* from miRBase (release 21), in the latter mature miRNAs with identical sequences were collapsed into single miRNAs; and the *A. thaliana* genome. For the differential expression analysis of the miRNAs, only reads mapping to the full-length mature miRNAs were considered, and primary alignments of reads mapping to the sense strand were counted (filtering with “samtools view-F 272”). Counts per miRNA were used as input for baySeq (version 2.14.0) to perform the differential expression analysis.

For this, miRNAs with low expression levels (less than five counts in all samples) were discarded, and size factors for each sample were set according to the total number of reads with length 24 nt or less mapping to the genome. Statistical analyses were performed in the R statistical programming environment (R Core Team, 2018) and graphics were produced with the ggplot package.

mRNA libraries were prepared with an in-house scaled-down version of Illumina's Tru-seq reaction. Briefly, Trizol total RNA was purified with NEBNext Poly(A) magnetic isolation Module (New England Biolabs, Ipswich, MA, USA), and heat fragmentated with Elute-Prime-Fragment buffer (5X first-strand buffer, 50 ng/mL random primers). Both first- and second-strand synthesis were performed with SuperScript II Reverse Transcriptase (ThermoFisher) and DNA polymerase I (NEB), respectively. End repair was done with T4 DNA polymerase, Klenow DNA polymerase and T4 Polynucleotide Kinase (NEB). A-tailing was performed with Klenow Fragment (3´→ 5´ exo-) (NEB). Universal adapters compatible with Nextera barcodes i7 and i5 (Rowan et al., 2017) were ligated with T4 DNA Ligase (NEB). PCR enrichment with using Nextera i7 and i5 barcodes was done with Q5 Polymerase (NEB). Purification of DNA in each step, and the size selection of the libraries prep were made with magnetic SPRI beads. Pair-end Illumina sequencing was performed with a HiSeq3000 apparatus. The detailed protocol is shown in Supplementary protocols. The analysis started with the trimming and filtering of reads using Trimmomatic (version 0.36, (Bolger et al., 2014)), setting the MAXINFO parameter to 90:04. Their quality was evaluated before and after trimming with FastQC (version 0.11.4, https://www.bioinformatics.babraham.ac.uk/projects/fastqc/) and MultiQC (Ewels et al., 2016). Reads were then mapped to the *A. thaliana* genome with STAR [version 2.5.2b, (Dobin et al., 2013)] and gene counts obtained with featureCounts (version 1.6.2). Finally, deferentially expressed genes were determined using DESeq2 (version 1.20.0) within the R statistical programming environment (R Core Team, 2018), filtering genes with 10 or less counts in all samples. Gene annotation was retrieved from Araport (Krishnakumar et al., 2015).

### Microscopy

Subcellular localization of HST and mutant versions of HST was observed in transgenic *A. thaliana* plants, while co-localization, BiFC or TriFC in transiently transformed *N. benthamiana* plants. GFP and RFP were excited at 480 nm or 552 nm, and emission was collected at 503 to 531 nm or 602 to 630 nm respectively. Citrine was excited at 514 nm and emission was collected at 525nm to 560nm. All assays were performed on a TCS SP8 confocal microscope (Leica, Solms, Germany). Nuclear/cytoplasmic GFP intensity ratios from hypocotyls of seven plants was quantified from forty images obtained from two different pools of plants with different insertion events of the different HST-GFP fusions. Density means of both cytoplasm and nucleus were measured by ImageJ, and the ratio between them was calculated.

### Author contribution

D.A.C., A.J.G, D.G and L.L. performed the experiments; W.Y. and D.S.L. developed the mRNA-seq protocol; A.L.A. analyzed the sequencing data; D.A.C, P.A.M., and D.W. conceived this study; P.A.M and D.W supervised the work and secured project funding; D.A.C., D.W., and P.A.M. wrote the manuscript.

### Acknowledgments

This work was supported by grants from ANPCyT (Agencia Nacional de Promoción Científica y Tecnológica, Argentina), HFSP (Human Frontier Science Program) and ICGEB (International Centre for Genetic Engineering and Biotechnology) to P.A.M and the Max Planck Society to P.A.M. and D.W. P.A.M. and A.L.A. are members of CONICET; D.A.C., A.J.G and D.G are fellows of the same institution. We thank the Deutscher Akademischer Austauschdienst (DAAD) for a short-term fellowship to D.A.C. In memory of Héctor Q. Manavella, who inspired his son P.A.M to become a scientist and passed away during the revision of this paper, one among many victims of Covid-19 infection.

## References


Achkar, N.P., Cambiagno, D.A., and Manavella, P.A. (2016). miRNA Biogenesis: A Dynamic Pathway. Trends in plant science 21:1034-1044.

Allen, R.S., Nakasugi, K., Doran, R.L., Millar, A.A., and Waterhouse, P.M. (2013). Facile mutant identification via a single parental backcross method and application of whole genome sequencing based mapping pipelines. Frontiers in plant science 4:362.

Baranauske, S., Mickute, M., Plotnikova, A., Finke, A., Venclovas, C., Klimasauskas, S., and Vilkaitis, G. (2015). Functional mapping of the plant small RNA methyltransferase: HEN1 physically interacts with HYL1 and DICER-LIKE 1 proteins. Nucleic acids research 43:2802-2812.

Bolger, A.M., Lohse, M., and Usadel, B. (2014). Trimmomatic: a flexible trimmer for Illumina sequence data. Bioinformatics 30:2114-2120.

Bollman, K.M., Aukerman, M.J., Park, M.Y., Hunter, C., Berardini, T.Z., and Poethig, R.S. (2003). HASTY, the Arabidopsis ortholog of exportin 5/MSN5, regulates phase change and morphogenesis. Development 130:1493-1504.

Bologna, N.G., Iselin, R., Abriata, L.A., Sarazin, A., Pumplin, N., Jay, F., Grentzinger, T., Dal Peraro, M., and Voinnet, O. (2018). Nucleo-cytosolic Shuttling of ARGONAUTE1 Prompts a Revised Model of the Plant MicroRNA Pathway. Molecular cell 69:709-719 e705.

Brownawell, A.M., and Macara, I.G. (2002). Exportin-5, a novel karyopherin, mediates nuclear export of double-stranded RNA binding proteins. The Journal of cell biology 156:53-64.

Cox, J., and Mann, M. (2008). MaxQuant enables high peptide identification rates, individualized p.p.b.-range mass accuracies and proteome-wide protein quantification. Nature biotechnology 26:1367-1372.

Cox, J., Neuhauser, N., Michalski, A., Scheltema, R.A., Olsen, J.V., and Mann, M. (2011). Andromeda: a peptide search engine integrated into the MaxQuant environment. Journal of proteome research 10:1794-1805.

Cui, Y., Fang, X., and Qi, Y. (2016). TRANSPORTIN1 Promotes the Association of MicroRNA with ARGONAUTE1 in Arabidopsis. The Plant cell 28:2576-2585.

774 Dalmadi, A., Gyula, P., Bálint, J., Szittya, G., and Havelda, Z. (2019). AGO-
775 unbound cytosolic pool of mature miRNAs in plant cells reveals a novel
776 regulatory step at AGO1 loading. Nucleic Acids Res 47: 9803–9817.
777 de Felippes, F.F., and Weigel, D. (2010). Transient assays for the analysis of
778 miRNA processing and function. Methods Mol Biol 592:255-264.
779 Dobin, A., Davis, C.A., Schlesinger, F., Drenkow, J., Zaleski, C., Jha, S., Batut,
780 P., Chaisson, M., and Gingeras, T.R. (2013). STAR: ultrafast universal
781 RNA-seq aligner. Bioinformatics 29:15-21.
782 Dolan, W.L., and Chapple, C. (2017). Conservation and Divergence of Mediator
783 Structure and Function: Insights from Plants. Plant & cell physiology
784 58:4-21.
785 Ewels, P., Magnusson, M., Lundin, S., and Kaller, M. (2016). MultiQC:
786 summarize analysis results for multiple tools and samples in a single
787 report. Bioinformatics 32:3047-3048.
788 Fang, X., Cui, Y., Li, Y., and Qi, Y. (2015). Transcription and processing of
789 primary microRNAs are coupled by Elongator complex in Arabidopsis.
790 Nature plants 1:15075.
791 Francisco-Mangilet, A.G., Karlsson, P., Kim, M.H., Eo, H.J., Oh, S.A., Kim, J.H.,
792 Kulcheski, F.R., Park, S.K., and Manavella, P.A. (2015). THO2, a core
793 member of the THO/TREX complex, is required for microRNA production
794 in Arabidopsis. The Plant journal : for cell and molecular biology 82:1018-
795 1029.
796 Guo, W., Liew, J.Y., and Yuan, Y.A. (2014). Structural insights into the arms
797 race between host and virus along RNA silencing pathways in
798 Arabidopsis thaliana. Biological reviews of the Cambridge Philosophical
799 Society 89:337-355.
800 Kalvari, I., Nawrocki, E.P., Argasinska, J., Quinones-Olvera, N., Finn, R.D.,
801 Bateman, A., and Petrov, A.I. (2018). Non-Coding RNA Analysis Using
802 the Rfam Database. Curr Protoc Bioinformatics 62:e51.
803 Kim, Y.J., Zheng, B., Yu, Y., Won, S.Y., Mo, B., and Chen, X. (2011). The role
804 of Mediator in small and long noncoding RNA production in Arabidopsis
805 thaliana. The EMBO journal 30:814-822.
806 Koiwa, H., Hausmann, S., Bang, W.Y., Ueda, A., Kondo, N., Hiraguri, A.,
807 Fukuhara, T., Bahk, J.D., Yun, D.J., Bressan, R.A., et al. (2004).

Arabidopsis C-terminal domain phosphatase-like 1 and 2 are essential Ser-5-specific C-terminal domain phosphatases. Proceedings of the National Academy of Sciences of the United States of America 101:14539-14544.

Kosugi, S., Hasebe, M., Tomita, M., and Yanagawa, H. (2009). Systematic identification of cell cycle-dependent yeast nucleocytoplasmic shuttling proteins by prediction of composite motifs. Proceedings of the National Academy of Sciences of the United States of America 106:10171-10176.

Krishnakumar, V., Hanlon, M.R., Contrino, S., Ferlanti, E.S., Karamycheva, S., Kim, M., Rosen, B.D., Cheng, C.Y., Moreira, W., Mock, S.A., et al. (2015). Araport: the Arabidopsis information portal. Nucleic acids research 43:D1003-1009.

Kurihara, Y., Takashi, Y., and Watanabe, Y. (2006). The interaction between DCL1 and HYL1 is important for efficient and precise processing of pri-miRNA in plant microRNA biogenesis. RNA 12:206-212.

Lang, P.L.M., Christie, M.D., Dogan, E.S., Schwab, R., Hagmann, J., van de Weyer, A.L., Scacchi, E., and Weigel, D. (2018). A Role for the F-Box Protein HAWAIIAN SKIRT in Plant microRNA Function. Plant physiology 176:730-741.

Langmead, B., Trapnell, C., Pop, M., and Salzberg, S.L. (2009). Ultrafast and memory-efficient alignment of short DNA sequences to the human genome. Genome Biol 10:R25.

Li, S., Le, B., Ma, X., You, C., Yu, Y., Zhang, B., Liu, L., Gao, L., Shi, T., Zhao, Y., et al. (2016). Biogenesis of phased siRNAs on membrane-bound polysomes in Arabidopsis. eLife 5.

Lobbes, D., Rallapalli, G., Schmidt, D.D., Martin, C., and Clarke, J. (2006). SERRATE: a new player on the plant microRNA scene. EMBO reports 7:1052-1058.

Lucero, L.E., Manavella, P.A., Gras, D.E., Ariel, F.D., and Gonzalez, D.H. (2017). Class I and Class II TCP Transcription Factors Modulate SOC1-Dependent Flowering at Multiple Levels. Molecular plant 10:1571-1574.

Luo, Y., Wang, Z., Ji, H., Fang, H., Wang, S., Tian, L., and Li, X. (2013). An Arabidopsis homolog of importin beta1 is required for ABA response and

drought tolerance. The Plant journal : for cell and molecular biology 75:377-389.

Manavella, P.A., Hagmann, J., Ott, F., Laubinger, S., Franz, M., Macek, B., and Weigel, D. (2012). Fast-forward genetics identifies plant CPL phosphatases as regulators of miRNA processing factor HYL1. Cell 151:859-870.

Manavella, P.A., Koenig, D., Rubio-Somoza, I., Burbano, H.A., Becker, C., and Weigel, D. (2013). Tissue-specific silencing of Arabidopsis SU(VAR)3-9 HOMOLOG8 by miR171a. Plant physiology 161:805-812.

Manavella, P.A., Yang, S.W., and Palatnik, J. (2019). Keep calm and carry on: miRNA biogenesis under stress. The Plant journal : for cell and molecular biology 99:832-843.

Meier, I., and Brkljacic, J. (2010). The Arabidopsis nuclear pore and nuclear envelope. The arabidopsis book 8:e0139.

Merkle, T. (2011). Nucleo-cytoplasmic transport of proteins and RNA in plants. Plant cell reports 30:153-176.

Mi, H., Muruganujan, A., Ebert, D., Huang, X., and Thomas, P.D. (2019). PANTHER version 14: more genomes, a new PANTHER GO-slim and improvements in enrichment analysis tools. Nucleic acids research 47:D419-D426.

Park, M.Y., Wu, G., Gonzalez-Sulser, A., Vaucheret, H., and Poethig, R.S. (2005). Nuclear processing and export of microRNAs in Arabidopsis. Proceedings of the National Academy of Sciences of the United States of America 102:3691-3696.

Peragine, A., Yoshikawa, M., Wu, G., Albrecht, H.L., and Poethig, R.S. (2004). SGS3 and SGS2/SDE1/RDR6 are required for juvenile development and the production of trans-acting siRNAs in Arabidopsis. Genes & development 18:2368-2379.

Qi, Y., Denli, A.M., and Hannon, G.J. (2005). Biochemical specialization within Arabidopsis RNA silencing pathways. Molecular cell 19:421-428.

Rogers, K., and Chen, X. (2013). Biogenesis, turnover, and mode of action of plant microRNAs. The Plant cell 25:2383-2399.

873 Rowan, B.A., Seymour, D.K., Chae, E., Lundberg, D.S., and Weigel, D. (2017).
874 Methods for Genotyping-by-Sequencing. Methods Mol Biol 1492:221-
875 242.
876 Telfer, A., and Poethig, R.S. (1998). HASTY: a gene that regulates the timing of
877 shoot maturation in Arabidopsis thaliana. Development 125:1889-1898.
878 Tomassi, A.H., Re, D.A., Romani, F., Cambiagno, D.A., Gonzalo, L., Moreno,
879 J.E., Arce, A.L., and Manavella, P.A. (2020). The Intrinsically Disordered
880 Protein CARP9 Bridges HYL1 to AGO1 in the Nucleus to Promote
881 MicroRNA Activity. Plant physiology 184:316-329.
882 Ueno, Y., Ishikawa, T., Watanabe, K., Terakura, S., Iwakawa, H., Okada, K.,
883 Machida, C., and Machida, Y. (2007). Histone deacetylases and
884 ASYMMETRIC LEAVES2 are involved in the establishment of polarity in
885 leaves of Arabidopsis. The Plant cell 19:445-457.
886 Vernoud, V., Horton, A.C., Yang, Z., and Nielsen, E. (2003). Analysis of the
887 small GTPase gene superfamily of Arabidopsis. Plant physiology
888 131:1191-1208.
889 Wang, J., Lee, J.E., Riemondy, K., Yu, Y., Marquez, S.M., Lai, E.C., and Yi, R.
890 (2020). XPO5 promotes primary miRNA processing independently of
891 RanGTP. Nature communications 11:1845.
892 Wang, S., Quan, L., Li, S., You, C., Zhang, Y., Gao, L., Zeng, L., Liu, L., Qi, Y.,
893 Mo, B., et al. (2019). The PROTEIN PHOSPHATASE4 Complex
894 Promotes Transcription and Processing of Primary microRNAs in
895 Arabidopsis. The Plant cell 31:486-501.
896 Wang, W., Ye, R., Xin, Y., Fang, X., Li, C., Shi, H., Zhou, X., and Qi, Y. (2011a).
897 An importin beta protein negatively regulates MicroRNA activity in
898 Arabidopsis. The Plant cell 23:3565-3576.
899 Wang, X., Xu, X., Ma, Z., Huo, Y., Xiao, Z., Li, Y., and Wang, Y. (2011b).
900 Dynamic mechanisms for pre-miRNA binding and export by Exportin-5.
901 RNA 17:1511-1528.
902 Wu, C., Li, X., Guo, S., and Wong, S. (2016). Analyses of RNA-Seq and sRNA-
903 Seq data reveal a complex network of anti-viral defense in TCV-infected
904 Arabidopsis thaliana. Sci Rep 6.

Wu, F.H., Shen, S.C., Lee, L.Y., Lee, S.H., Chan, M.T., and Lin, C.S. (2009). Tape-Arabidopsis Sandwich - a simpler Arabidopsis protoplast isolation method. Plant methods 5:16.

Yamazawa, R., Jiko, C., Choi, S., Park, I.Y., Nakagawa, A., Yamashita, E., and Lee, S.J. (2018). Structural Basis for Selective Binding of Export Cargoes by Exportin-5. Structure 26:1393-1398 e1392.

Zhang, B., You, C., Zhang, Y., Zeng, L., Hu, J., Zhao, M., Chen, X., (2020). Linking key steps of microRNA biogenesis by TREX-2 and the nuclear pore complex in Arabidopsis. Nat Plants 6:957-969.

Zhang, X., Henriques, R., Lin, S.S., Niu, Q.W., and Chua, N.H. (2006). Agrobacterium-mediated transformation of Arabidopsis thaliana using the floral dip method. Nature protocols 1:641-646.

Zhang, X., Jayaweera, D., Peters, J.L., Szecsi, J., Bendahmane, M., Roberts, J.A., and Gonzalez-Carranza, Z.H. (2017a). The Arabidopsis thaliana F-box gene HAWAIIAN SKIRT is a new player in the microRNA pathway. PloS one 12:e0189788.

Zhang, Z., Guo, X., Ge, C., Ma, Z., Jiang, M., Li, T., Koiwa, H., Yang, S.W., and Zhang, X. (2017b). KETCH1 imports HYL1 to nucleus for miRNA biogenesis in Arabidopsis. Proceedings of the National Academy of Sciences of the United States of America 114:4011-4016.

Zhu, J., Li, Y., Lin, J., Wu, Y., Guo, H., Shao, Y., Wang, F., Wang, X., Mo, X., Zheng, S., et al. (2019). CRD1, an Xpo1 domain protein, regulates miRNA accumulation and crown root development in rice. The Plant journal : for cell and molecular biology.

**Figure legends**

**Figure 1. HST does not participate in the nucleus-cytoplasm export of miRNAs.** (A) RNA blot of total, nuclear, and cytoplasmic RNA extracted from 15 days wild type (Col-0) and *hst-15*. (B) RNA blot of total miRNAs in Col-0 wild-type, *ran* single and double mutant plants. (C) Relative quantification of RNA blot replicates showing nucleus/cytoplasm miRNA content in *ran* single and double mutants, *ago1* mutants, and *hst-15* mutants transformed with $HST^{\Delta N}$. ImageJ was used to quantify the intensity of the bands and values were normalized to Col-0 (red line). One representative experiment from three

independent assays is shown. RNA blots used to calculate the ratios are shown in Figure 1B and 3E, Supplemental Figure 1G. The same ratios were calculated by RT-qPCR and displayed in Supplemental Figure 1C. (D-E) Total miRNA levels in Col-0, *hst-15*, and *hst-15* transformed with *HST* or $HST^{\Delta N}$ quantified by RNA blot (D) or RT-qPCR (E) ($P<0.01$ by one-way ANOVA followed by Tukey's multiple comparison test). For A, B, and D, U6 and tRNA were used as loading controls and as internal controls of nuclear and cytoplasmic fractions. In each case, the band intensity, quantified using ImageJ and normalized, was normalized to corresponding RNA-fraction of Col-0 plants.

**Figure 2. HST sub-cellular distribution relies on its N-terminal domain and RAN1.** (A) GFP:HST sub-cellular localization in wild-type Col-0 plants leaves expressing *35S:GFP:HST*. (B) Nuclear/cytoplasmic distribution of GFP:HST, GFP:$HST^{\Delta N}$ or GFP:$HST^{\Delta C}$ expressed under the 35S promoter in hypocotyls of Col-0 wild-type and *ran* single or double mutant plants as observed by confocal microscopy. (C) Quantification of the GFP intensity in the nucleus and cytoplasm of cells displayed in (B). GFP intensity was measured with ImageJ. Different letters indicate a significant difference ($P<0.01$ by one-way ANOVA followed by Tukey's multiple comparison test). (D) Epithelial cell of *N. benthamiana* plants transformed with 35S:mCherry:HST and either 35S:eGFP:$HST^{\Delta C}$ or 35S:eGFP:$HST^{\Delta N}$. The white line in the image indicates transects where red and green signals were measured by ImageJ and plotted in the histograms. (E) Schematic representation of the truncated versions of HST fused to eGFP. Yellow lines mark the position of two predicted NLS (271-300 bp, and 355-387 bp). Both NLSs are compatible with nuclear/cytoplasmic shuttling proteins having scores of 4.6 and 5.1 respectively as predicted with "cNLS Mapper" (Kosugi et al., 2009). (F) Sub-cellular localization of HST and different truncated versions of HST in leaves of *A. thaliana* transgenic plants expressing GFP:HST or GFP GFP:$HST^{\Delta N}$ [Δ1-107(Bollman et al., 2003)], GFP:$HST^{\Delta N322}$ (Δ1-322) and GFP:$HST^{\Delta C}$ (Δ963-1202). All scale bars represent 20 μm. In all cases constructs were cloned under the 35S promoter.

**Figure 3. Nuclear import of HST requires its interaction with IMPA-2.** (A) BiFC assay performed in *N. benthamiana* plants co-transformed with either

HST:N-mCitrine or HST$^{\Delta N}$:N-mCitrine and IMPA-2:C-mCitrine. CARP9, a nuclear protein acting in late steps of miRNA pathway (Tomassi et al., 2020), was used as negative control. Additional positive and negative controls for the BIFC assays are shown in Supplemental Figure 4. (B) Nuclear/cytoplasmic distribution of 35S:GFP:HST and 35S:GFP:HST$^{\Delta N}$ in hypocotyls of Col-0 and *impa-2* mutant plants as observed by confocal microscopy. All scale bars represent 20 μm. White arrow indicates a positive nucleus quantified in (D). (C) Percentage of cells, in Col-0 and *impa-2* mutant backgrounds, with detectable GFP signal in the nucleus. One representative experiment from two different assays is shown. (D) Quantification of the GFP intensity in the nucleus and cytoplasm of cells displayed in (B). GFP intensity was measured with ImageJ. Different letters indicate a significant difference ($P<0.05$ by two-way ANOVA followed by Bonferroni correction for multiple comparisons). (E) RT-qPCR quantification of mature miRNAs in total RNA extracted from 15 days old wild type (Col-0), *hst-15,* and *impa-2* mutants. Differences between samples with a $P<0.05$ (**) or $<0.01$ (*), in a two-tailed unpaired T-Test, were considered statistically significant. (F) RNA blot of total, nuclear and cytoplasmic RNA extracted from 15 days wild type (Col-0), *impa-2* mutants, and *hst-15* plants either transformed or not with a 35S:GFP:HST$^{\Delta N}$. U6 and tRNA were used as internal controls of nuclear and cytoplasmic fractions. Bands intensities were quantified using ImageJ and expressed as relative to corresponding RNA-fraction of Col-0 plants.

**Figure 4. HST influences miRNA biogenesis, but it is not directly involved in pri-miRNA processing.** (A) Box plot showing a genome-wide analysis of miRNA levels in Col-0 wild type, *hst-15,* and *hst-15* transformed with *35S:GFP:HST* or *35S:GFP:HST$^{\Delta N}$*. (B) Scatter plot comparing the counts per million +1 (log scale) of miRNAs between Wild type (Col-0) and *hst-15* mutants transformed or not with 35S:GFP:HST or 35S:GFP:HST$^{\Delta N}$.(C) MiRNAs reduced activated in two or more miRNA related mutants. Members of single miRNAs families with identical sequence were collapsed as single miRNAs. The intersection size indicates the number of miRNAs repressed in a given group of mutants noted as grey dots join by a line. Set size indicates the total number of repressed miRNAs families in a sample. (D) Box plot from RNA-seq analysis of

pri-miRNAs and miRNA-target genes levels in *hst-15* relative to Col-0 plants. (E) Scatter plot and Pearson correlation comparing the log2 fold change of pri-miRNAs between pair of mutants (red line mark 0). mRNA-seq of *dcl1-9*, *hyl1-2*, *cpl1/2* and *se-3* were obtained from available mRNA-seq (Manavella et al., 2012; Wu et al., 2016). (F) *In vitro* processing of pri-amiRLUC by equal amounts of protein extracts from *dcl1-100*, Col-0, and *hst-15* samples. Processing activity was measured by quantifying the produced mature amiRLUC by RT-qPCR and expressed relative to *dcl1-100* samples. (G) Pri-miRNA association with HST was assayed by RIP assay using an αGFP antibody on plants expressing GFP:HST. As a positive control, HYL1-associated pri-miRNAs were measured (IP αHYL1) in the same plants. IP using an αGFP antibody in plants expressing GFP was used as a negative control (red line). (H-I) Transcript and protein levels of AGO1, SE, HYL1, DCL1, and or HEN assayed by protein blot and RT-qPCR, respectively. Relative transcript levels were obtained by the $2^{-\Delta\Delta Ct}$ method comparing each gene with ACTIN7/8 and values obtained in wild-type Col-0 plants. (J) RIP-RT-qPCR experiment to quantify HST-associated mature miRNAs. The experiment was performed using anti-GFP antibody on plants expressing GFP:HST or GFP:HST$^{\Delta N}$. Plants expressing GFP were used for a negative control (red line). In all panels, an asterisk marks a significant difference of P<0.01, by one-way ANOVA test followed by Tukey's multiple comparison test.

**Figure 5. DCL1 recruitment to *MIR* genes depends on its interaction with HST.** (A and C) BiFC assays of *N. benthamiana* leaves showing the interaction of HST (A) or HST$^{\Delta N}$ (C) with DCL1, HYL1, SE or CPL1. Negative interacting controls are shown in Supplemental Figure 4A. (B) Y2H assay testing the interaction between HST and HYL1, SE, CPL1, HST, HEN1, or DCL1. Input samples were grown in –LT medium, while the interactions between proteins were detected when yeast are grown in –LTH with 10 mM 3-AT. (D) BiFC and TriFC showing DCL1-MED37-D and DCL1-MED37-E interaction in *N. benthamiana* leaves in the presence or absence of HST, respectively. Quantification of nuclear GFP intensity of 100 nuclei was performed with ImageJ and plotted on the right side of representative images. Double asterisks mark a significant difference of P<0.01 in a two tailed,

unpaired, *t*-test corrected with FDR < 0.01 for multiple pair comparisons. All scale bars represent 10 μm (E-G) MED37:GFP-, HST:GFP-, and DCL1-Chromatin association, as measured by ChIP-qPCR assays. Anti-IgG antibody was used in each sample as a negative control (red line). (H) HYL1 association to pri-miRNA as measure by RIP-qPCR assays in Col-0 and *hst-15* mutants. Anti-IgG antibody was used in each sample as a negative control (red line) along with samples extracted from *hyl1-2* mutants. Differences between samples with a P<0.05 (*) or <0.01 (**), by one-way ANOVA followed by Tukey's multiple comparison test, were considered statistically significant.

**Figure 6. Independent functions of HST as a cargo-translocation protein and as miRNA biogenesis factor.** HST interacts with MED37 sub-units and acts as a scaffold to recruit DCL1 to *MIRNA* loci. This interaction could allow the initial assembly of the processing complex at co-transcriptional level. After miRNA processing by DCL1, an enzymatic activity not reliant on HST, mature miRNAs are likely translocated to the cytoplasm associated with AGO1 (Bologna et al., 2018). Independently, HST may act as a karyopherin for the translocation of cargoes from the nucleus and cytoplasm, when interacting with RAN1, and from the cytoplasm to the nucleus when interacting with IMPA-2. The cycle of import-export of HST may be complete by HST-IMPA-2 interaction.

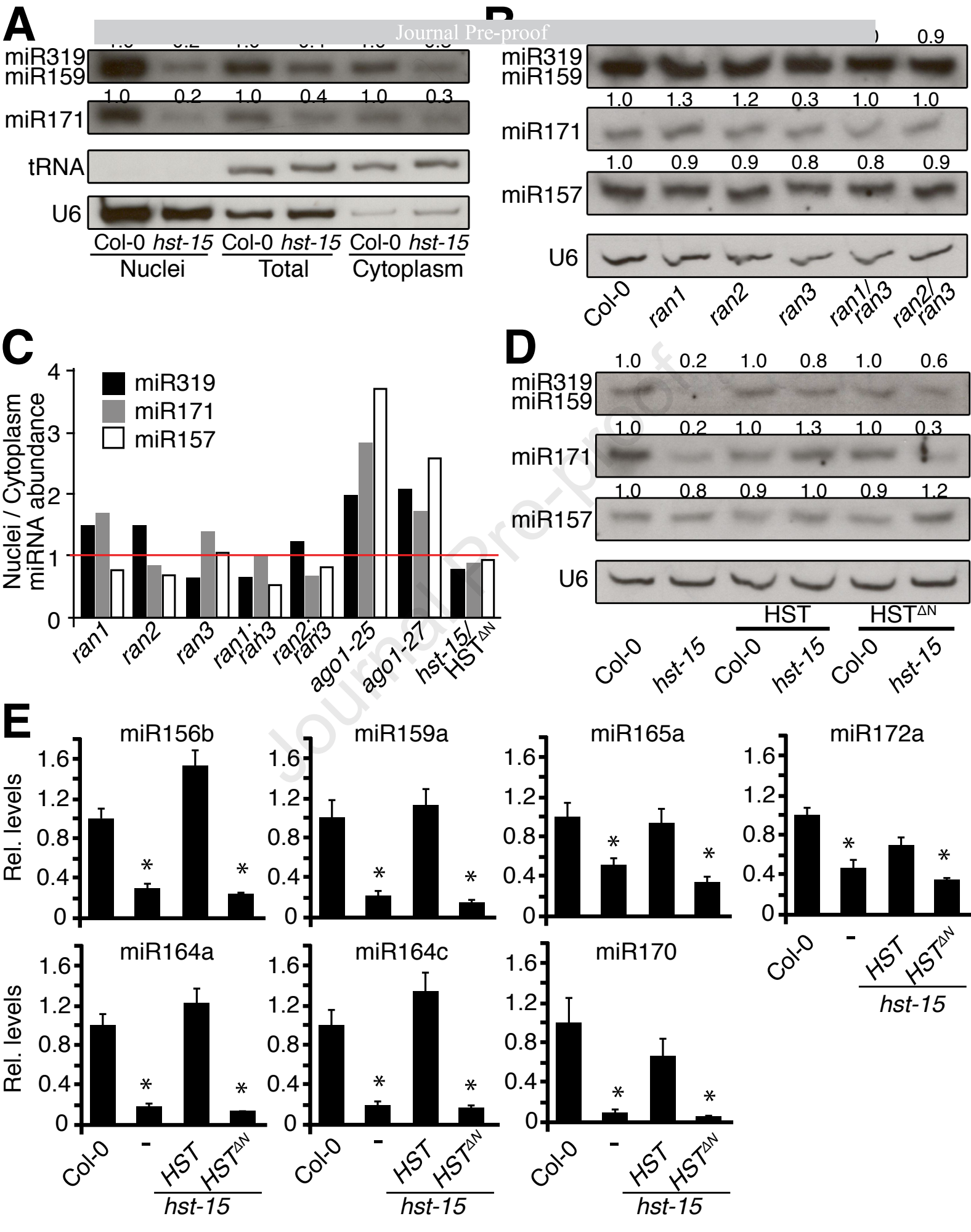

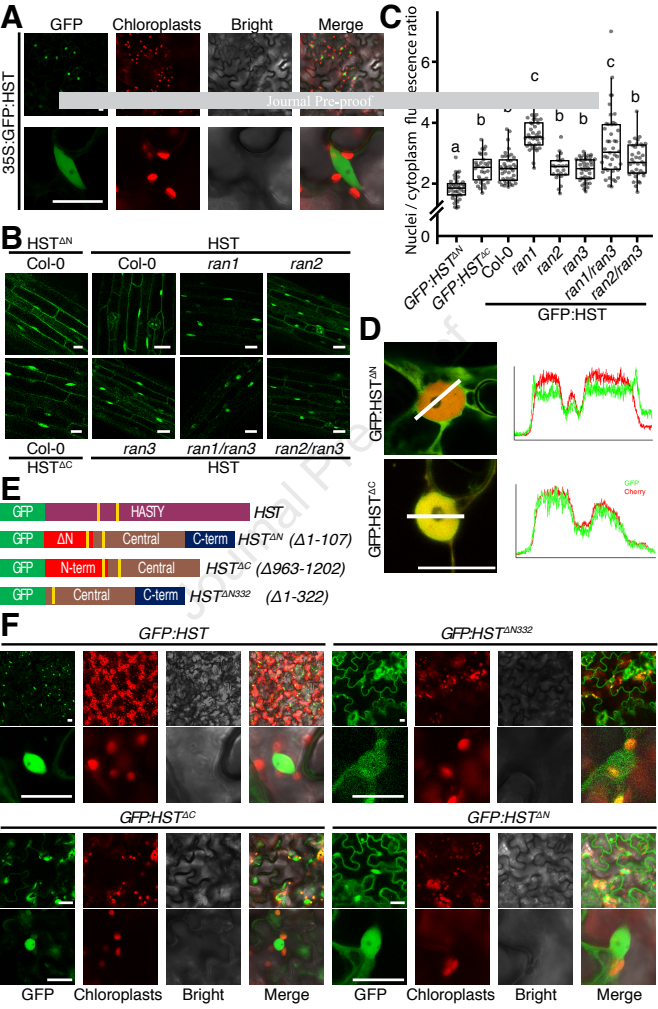
A
GFP
Chloroplasts
Bright
Merge
35S:GFP:HST
Journal Pre-proof
C
Nuclei / cytoplasm fluorescence ratio
a
b
b
c
b
b
c
b
GFP:HST^ΔN
GFP:HST^ΔC
Col-0
ran1
ran2
ran3
ran1/ran3
ran2/ran3
GFP:HST
B
HST^ΔN
HST
Col-0
Col-0
ran1
ran2
ran3
ran1/ran3
ran2/ran3
HST^ΔC
HST
D
GFP:HST^ΔN
GFP:HST^ΔC
GFP
Cherry
E
GFP
HASTY
HST
GFP
ΔN
Central
C-term
HST^ΔN (Δ1-107)
GFP
N-term
Central
HST^ΔC (Δ963-1202)
GFP
Central
C-term
HST^ΔN332 (Δ1-322)
F
GFP:HST
GFP:HST^ΔN332
GFP:HST^ΔC
GFP:HST^ΔN
GFP
Chloroplasts
Bright
Merge
GFP
Chloroplasts
Bright
Merge

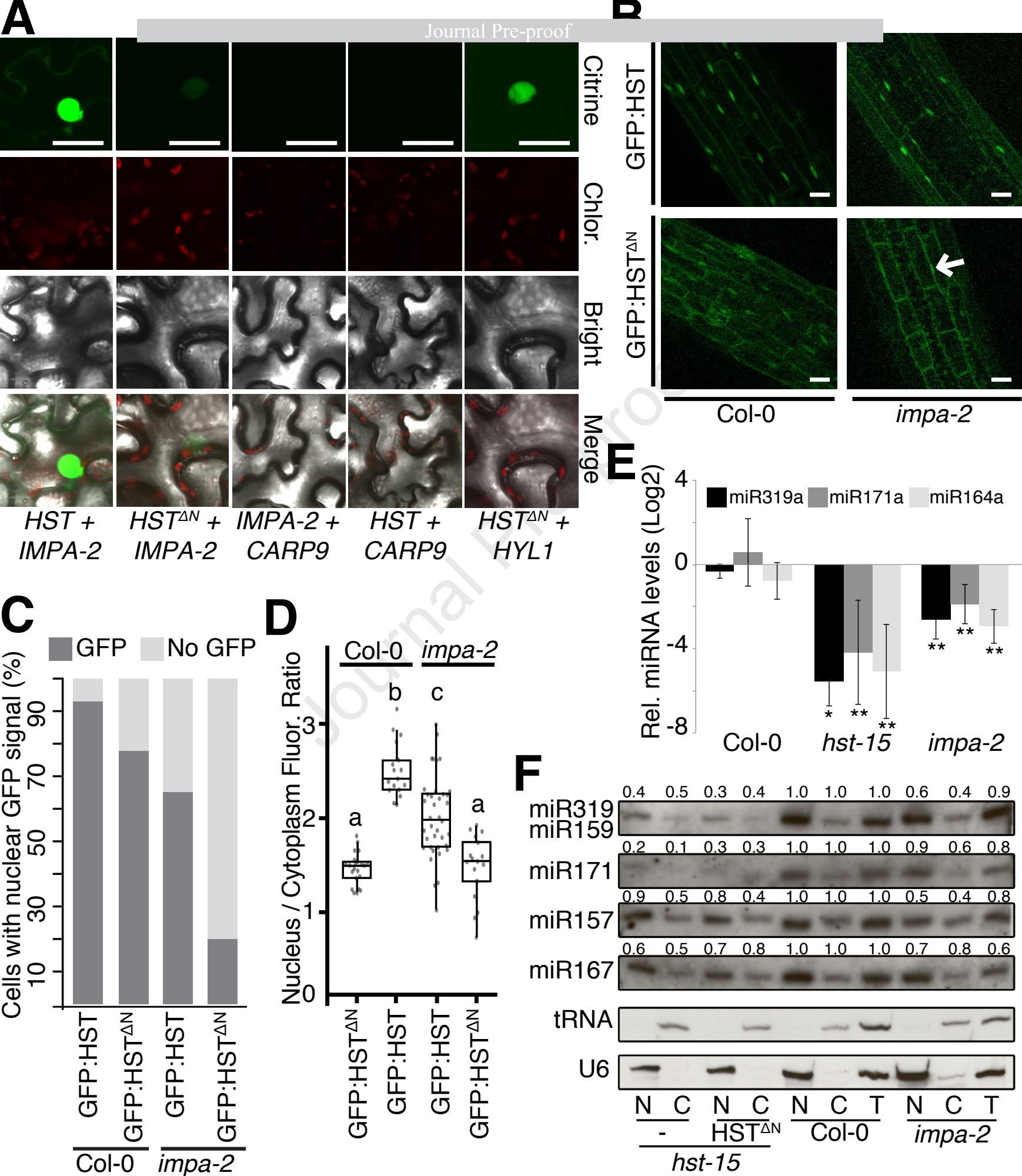

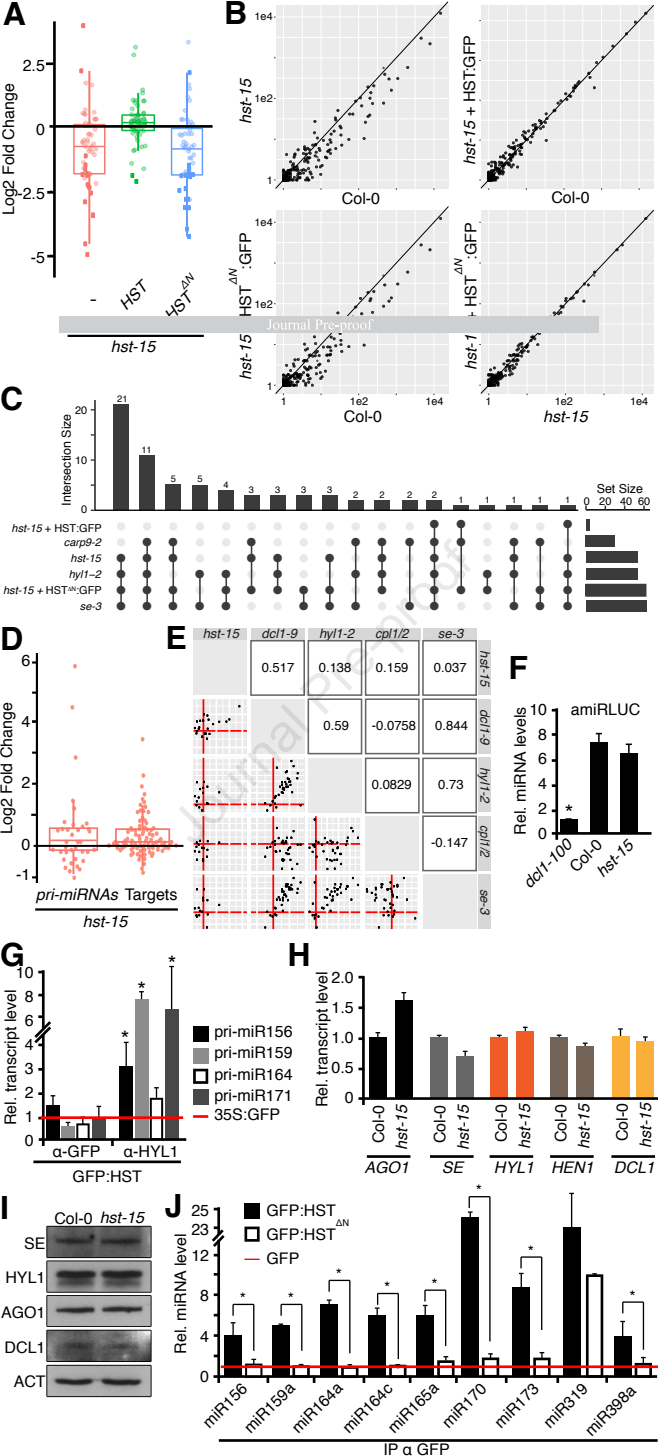
A
Log2 Fold Change
2.5
0
-2.5
-5
-
HST
HST^ΔN
hst-15
B
hst-15
Col-0
hst-15 + HST:GFP
HST^ΔN:GFP
hst-1
Journal Preproof
C
Intersection Size
21
11
5
5
4
3
3
3
3
2
2
2
2
1
1
1
1
1
Set Size
0 20 40 60
hst-15 + HST:GFP
carp9-2
hst-15
hyl1-2
hst-15 + HST^ΔN:GFP
se-3
D
Log2 Fold Change
pri-miRNAs
Targets
hst-15
E
hst-15
dcl1-9
hyl1-2
cpl1/2
se-3
0.517
0.138
0.159
0.037
0.59
-0.0758
0.844
0.0829
0.73
-0.147
F
amiRLUC
Rel. miRNA levels
dcl1-100
Col-0
hst-15
G
Rel. transcript level
pri-miR156
pri-miR159
pri-miR164
pri-miR171
35S:GFP
α-GFP
α-HYL1
GFP:HST
H
Rel. transcript level
Col-0
hst-15
AGO1
SE
HYL1
HEN1
DCL1
I
Col-0
hst-15
SE
HYL1
AGO1
DCL1
ACT
J
Rel. miRNA level
GFP:HST
GFP:HST^ΔN
GFP
miR156
miR159a
miR164a
miR164c
miR165a
miR170
miR173
miR319
miR398a
IP α GFP

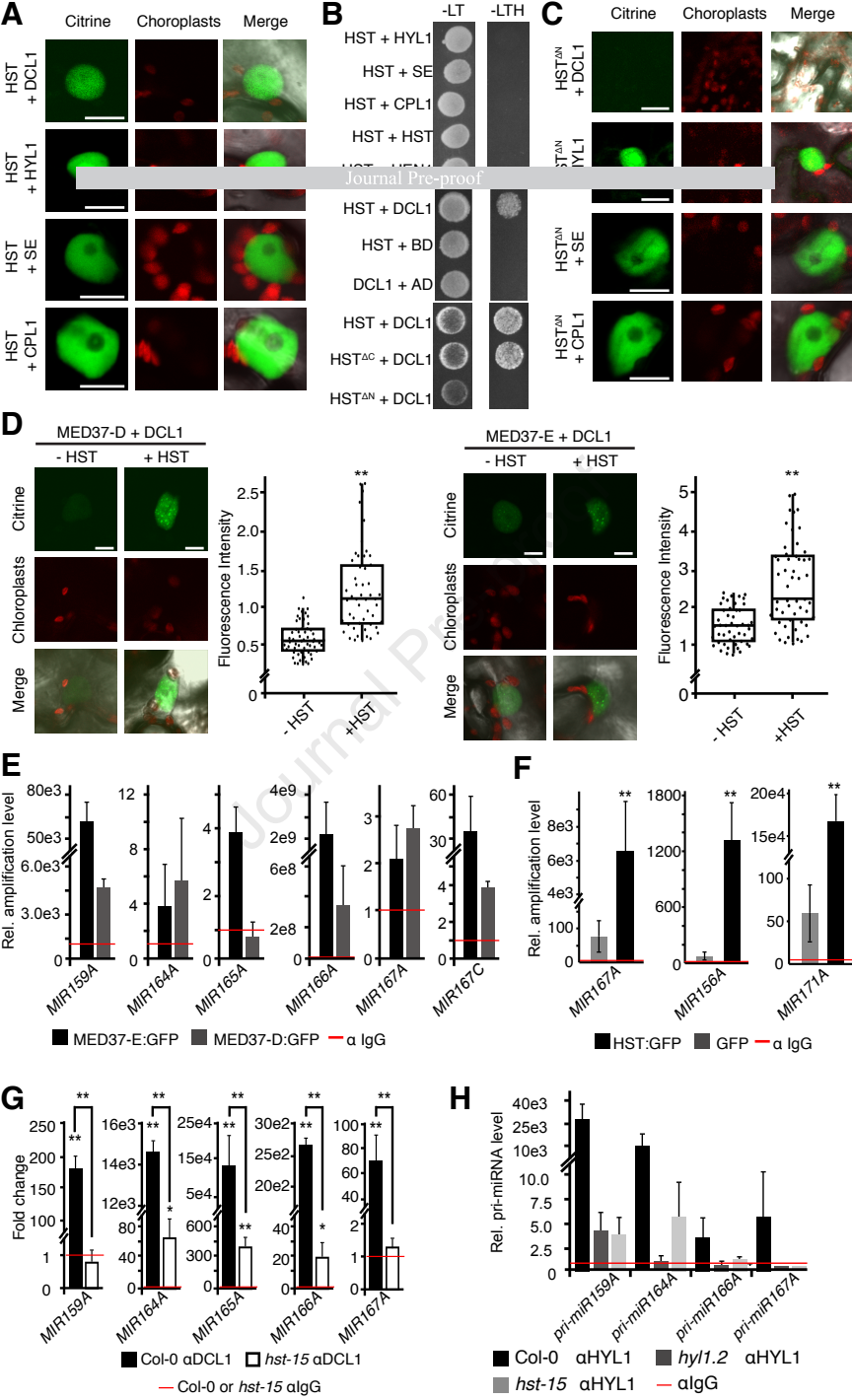
A
Citrine
Choroplasts
Merge
HST + DCL1
HST + HYL1
HST + SE
HST + CPL1
B
-LT
-LTH
HST + HYL1
HST + SE
HST + CPL1
HST + HST
HST + DCL1
HST + BD
DCL1 + AD
HST + DCL1
HST^ΔC + DCL1
HST^ΔN + DCL1
C
Citrine
Choroplasts
Merge
HST^ΔN + DCL1
HST^ΔN + SE
HST^ΔN + CPL1
Journal Pre-proof
D
MED37-D + DCL1
- HST
+ HST
Citrine
Chloroplasts
Merge
Fluorescence Intensity
- HST
+HST
MED37-E + DCL1
- HST
+ HST
Citrine
Chloroplasts
Merge
Fluorescence Intensity
- HST
+HST
E
Rel. amplification level
MIR159A
MIR164A
MIR165A
MIR166A
MIR167A
MIR167C
MED37-E:GFP
MED37-D:GFP
α IgG
F
Rel. amplification level
MIR167A
MIR156A
MIR171A
HST:GFP
GFP
α IgG
G
Fold change
MIR159A
MIR164A
MIR165A
MIR166A
MIR167A
Col-0 αDCL1
hst-15 αDCL1
Col-0 or hst-15 αIgG
H
Rel. pri-miRNA level
pri-miR159A
pri-miR164A
pri-miR166A
pri-miR167A
Col-0 αHYL1
hyl1.2 αHYL1
hst-15 αHYL1
αIgG